14

DETERMINATION OF THE PHASE CONSTANT OF CLOSED TRANSMISSION LINE SYSTEMS USING THE FINITE DIFFERENCE AND THE CONJUGATE GRADIENT METHOD

V. Narayanan and R. K. Lade

14.1 Introduction

The aim of this paper is to compute the characteristics (the phase constant β, the cutoff wave numbers and the field distributions) for the first few dominant modes of arbitarary shaped conducting and dielectric filled waveguide structures. Dispersion characteristics for the hybrid modes in inhomogenous shielded transmission line structures has been obtained.

The analysis would employ the finite difference technique. The resulting eigenvalue problem will then be solved iteratively using the conjugate gradient method.

Although transmission lines can be very simple in construction, they belong to a family of the so called inhomogenously filled waveguide

structures. This implies that no TEM or waveguide type TE or TM modes exist independently, making an accurate analysis difficult.

Over the past twentyfive years or so [1–16], a number of analytical numerical solutions to such problems have been suggested. A good approximation at low frequencies is the quasi-TEM analysis. Althogh useful, this method becomes increasingly inaccurate as the operating frequency is increased. The quasi-TEM analysis does not account for the hybrid nature of the guided modes and hence results in the inaccuracy. The dispersive nature of the structure cannot be predicted by the quasi-TEM method. Hence there is a need for a much rigorous full wave solution taking into consideration the various boundary conditions. The finite difference method proposed, involves such a full wave analysis.

For the solution of the modes in the waveguide structures, it is necessary to apply the finite difference technique to the operator equation. This results in solving an $N \times N$ matrix eigenvalue problem. This could be a limiting factor due to memory limitations in computers. However,this is overcome by observing that the system matrix is very sparse. Hence the information about an $N \times N$ system may be stored in an array of $N \times 8$ matrix with another $N \times 8$ matrix containing the column position of the elements. So one may drastically cut down on the memory requirements of the finite difference technique. Also the minimum eigenvalues of this sparse matrix are of interest because we are looking for the first few dominant modes. The conjugate gradient method takes advantage of this fact and solves iteratively for the lower few eigenvalues. Unlike the traditional methods in which all eigenvalues are found and the first few desired ones are selected, this method just finds the required eigenvalues. This results in a saving on computer time. Hence quite large problems with a few thousand unknowns may be solved quickly even on a desktop PC. The phase constant β can be obtained from the eigenvalues.

The eigenvectors corresponding to the desired eigenvalues for the TE, TM and hybrid mode equations give the electric and magnetic vector potentials inside the structure. Hence the various E and H field plots may be obtained from this information.

So one would have the complete solution for β of the first few dominant TE, TM and hybrid modes of arbitrary shaped conducting structures partially filled with dielectrics.

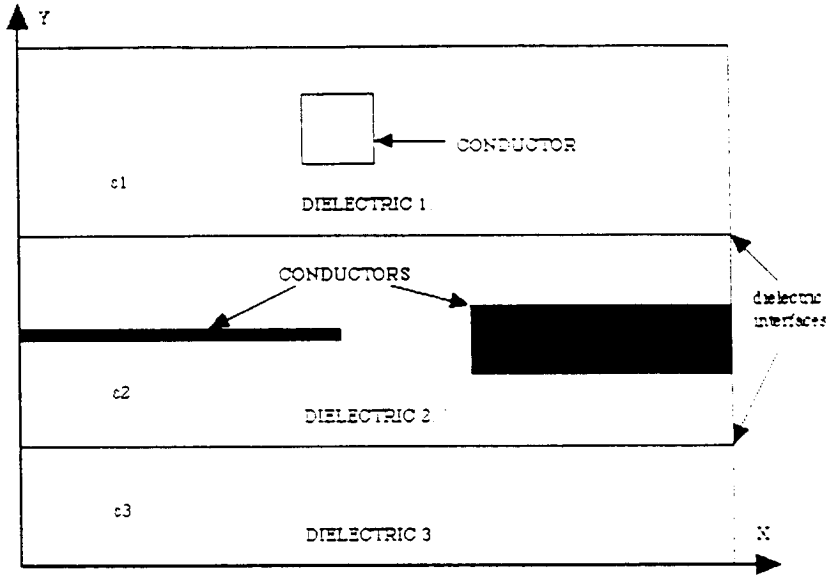

Figure 14.1 General closed transmission line configuration.

14.2 Problem Definition and Formulation

Consider the cross section of an arbitarary shaped waveguide structure as shown in Fig. 14.1. We assume that the system is uniform in the z-direction. The guided waves in the z-direction are of interest. The behavior in the z-direction is assumed to be exponential.(i.e. $e^{-j\beta z}$)

In the homogenous source free regions, Maxwell's equations may be written as

$$\overline{E} = -\overline{\nabla} \times \overline{F} - \hat{z}\overline{A} + \overline{\nabla}(\overline{\nabla} \cdot \overline{A})/\hat{y} \tag{1}$$

$$\overline{H} = \overline{\nabla} \times \overline{A} - \hat{y}\overline{F} + \overline{\nabla}(\overline{\nabla} \cdot \overline{F})/\hat{z} \tag{2}$$

where the magnetic vector potential $\overline{A}$ and the electric vector potential $\overline{F}$ satisfy

$$\nabla_t^2 \overline{A} + k^2 \overline{A} = 0 \tag{3}$$

$$\nabla_t^2 \overline{F} + k^2 \overline{F} = 0 \tag{4}$$

where ∇_t is the transverse derivative. It could now be shown that

$$\overline{F} = \overline{a}_z (k_c^2/\hat{y})\phi \tag{5}$$

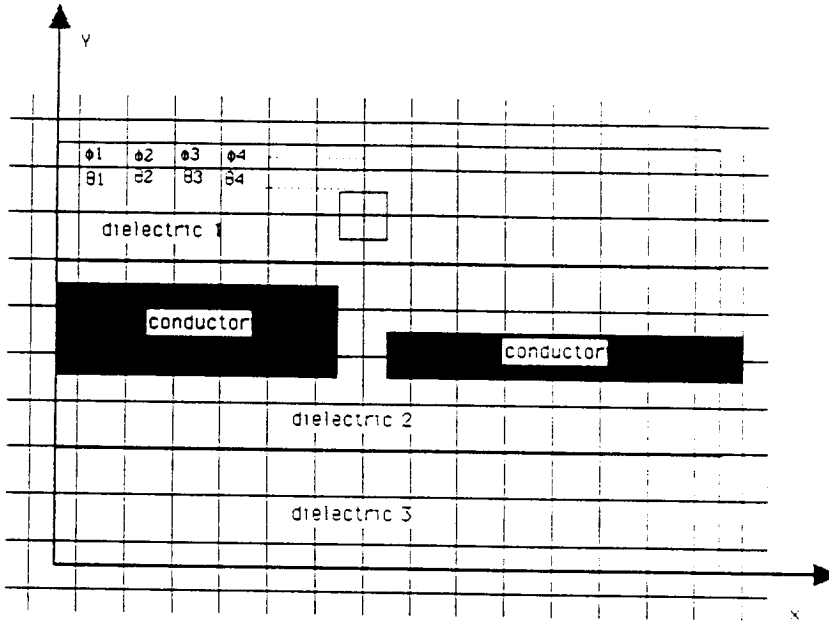

Figure 14.2 Finite difference mesh and labeling of ϕ and θ at each node.

for the TE field, and

$$\overline{A} = \overline{a}_z(\beta\hat{y}/\omega\epsilon_o k_c^2)\theta \tag{6}$$

for the TM field. Here $\hat{y} = \sigma_o + j\omega\epsilon_o$ and $\hat{z} = j\omega\mu_o$, k is the free space wave number, k_c is the cutoff wave number and $\overline{a}_z$ is the unit vector in the z-direction.

Assuming the fields in the z-direction to be of the form $exp(-j\beta z)$, we can reduce equations (1) and (2) to

$$E_x = (-j\beta^2/\omega\epsilon_o k_c^2)\delta\theta/\delta x - (j\omega\mu/k_c^2)\delta\phi/\delta y \tag{7}$$

$$E_y = (j\beta^2/\omega\epsilon_o k_c^2)\delta\theta/\delta y - (j\omega\mu/k_c^2)\delta\phi/\delta x \tag{8}$$

$$E_z = (\beta/\omega\epsilon_o)\theta \tag{9}$$

$$H_x = (j\beta\epsilon/k_c^2\epsilon_o)\delta\theta/\delta y - (j\beta/k_c^2)\delta\phi/\delta \tag{10}$$

$$H_y = (j\beta\epsilon/k_c^2\epsilon_o^2)\delta\theta/\delta x - (j\beta/k_c^2)\delta\phi/\delta y \tag{11}$$

$$H_z = \phi \tag{12}$$

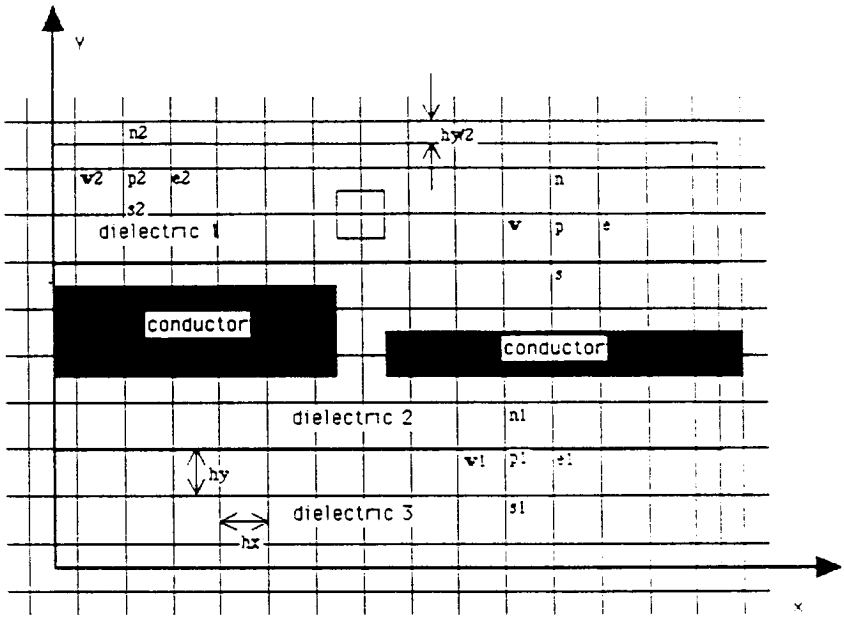

Figure 14.3 Nodes used for finite difference equation at any node P and boundary condition at node P^2.

The substitution of (5) and (6) in (3) and (4) results in

$$\nabla_t^2 \phi + k^2 \phi = 0 \tag{13}$$

$$\nabla_t^2 \theta + k^2 \theta = 0 \tag{14}$$

Making the substitution

$$\phi = \Phi(x, y) e^{-j\beta z} \tag{15}$$

$$\theta = \Theta(x, y) e^{-j\beta z} \tag{16}$$

one obtains

$$\nabla_t^2 \Phi + k_c^2 \Phi = 0 \tag{17}$$

$$\nabla_t^2 \Theta + k_c^2 \Theta = 0 \tag{18}$$

When the system contains more than one dielectric, the electric and magnetic potentials are coupled. Equation (17) and (18) have to be satisfied in each dielectric region. Define

$$\overline{\beta} = \frac{\beta}{k_o} \tag{19}$$

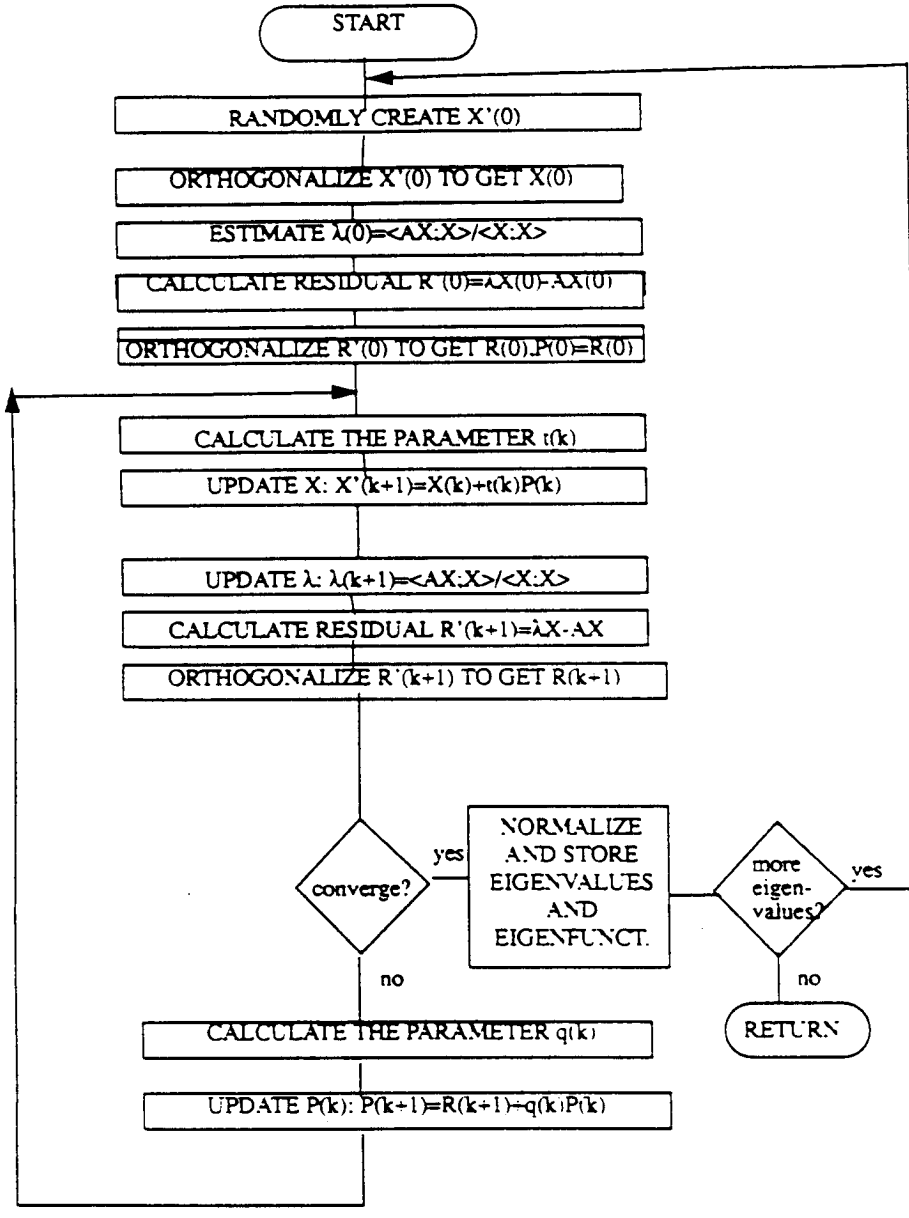

Figure 14.4 Flow chart for the conjugate gradient method.

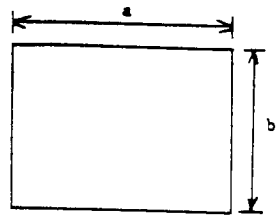

a=4.0
b=3.0

(a)

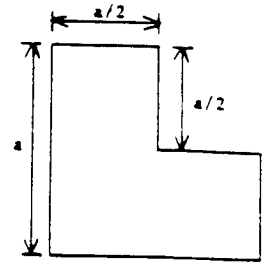

a=1.00

(b)

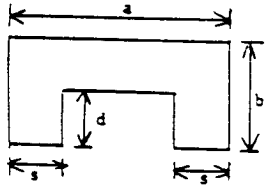

a=1.0 s=0.25
b=0.5 d=0.25

(c)

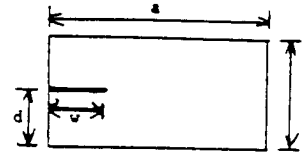

a=2.0 w=0.5
b=1.0 d=0.5

(d)

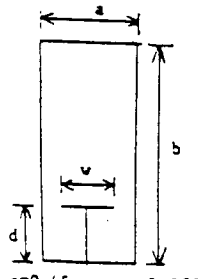

a=0.45 w=0.250
b=1.0 d=0.25

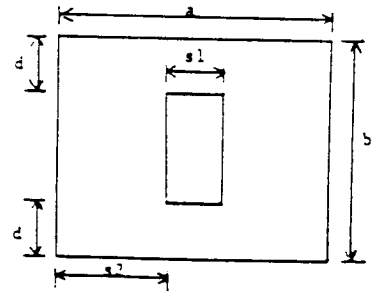

a=1.25 s1=0.250 s2=0.5
b=1.0 d=0.25

Figure 14.5 Configurations considered in section 14.5.1 (a) Rectangular waveguide, (b) L-shaped waveguide, (c) Single ridge waveguide, (d) Vaned rectangular waveguide, (e) T-Septate waveguide, (f) Coaxial rectangular waveguide.

and

$$k_{ci}^2 = \epsilon_{ri}\mu_{ri}k_o^2 - \beta^2 = k_i^2 - \beta^2 \tag{20}$$

where k_o is the free space wave number ($k_o^2 = \omega^2\epsilon_o\mu_o$) and k_i is the wave number in the i^{th} dielectric($k_i^2 = \omega^2\epsilon_i\mu_i$). So

$$\nabla_t^2\Phi + k_{ci}^2\Phi = 0 \tag{21}$$

$$\nabla_t^2\Theta + k_{ci}^2\Theta = 0 \tag{22}$$

which mathematically represents finding the eigen spectrum of the operator $-\nabla_t^2$. Defining τ_i as

$$\tau_i = \frac{1 - \overline{\beta}^2}{\epsilon_{ri}\mu_{ri} - \overline{\beta}^2} = \frac{k_{co}^2}{k_{ci}^2} \tag{23}$$

reduces the problem to

$$\tau_i\nabla_t^2\Phi + k_{co}^2\Phi = 0 \tag{24}$$

$$\tau_i\nabla_t^2\Theta + k_{co}^2\Theta = 0 \tag{25}$$

where

$$k_{co}^2 = k_o^2 - \beta^2 \tag{26}$$

For the TE field, ϕ is proportional to the longitudinal magnetic field. On the metallic walls, the Neumann's condition is met. Thus

$$\frac{\delta\Phi}{\delta n} = 0 \tag{27}$$

For the TM field, θ is proportional to the longitudinal electric field. Once again on the metalic walls the Dirichlet's boundary condition is met. Thus

$$\Theta = 0 \tag{28}$$

on the metallic walls.

On the dielectric to dielectric interfaces, the following boundary conditions are satisfied.

$$B_x^i = B_x^{i+1} \tag{29}$$

$$H_y^i = H_y^{i+1} \tag{30}$$

The eigenvalue found is equal to k_c^2. Hence we may find β using the relation

$$\beta^2 = k^2 - k_c^2 \tag{31}$$

Thus the characteristics of the arbitrary shaped waveguide are obtained.

14.3 Solution by Finite Difference Method

A fundamental approach for obtaining the numerical approximation of differential equations is the finite difference method.

This involves the following steps.

1) Covering the domain by a finite difference mesh.
2) Labelling the nodes suitably to represent the electric and magnetic vector potentials.
3) Determining the numerical solution at each node by applying the finite difference approximation to the linear differential equation.
4) Formulating the finite difference approximation for the boundary conditions at the appropriate nodes.
5) Solving the set of finite difference equations thus obtained to obtain the electric and magnetic vector potentials at the nodes.

The cross section is covered by a simple mesh. This is done in such a way that the grid lines are half a step size away from all the metal surfaces and such that they coincide with the dielectric to dielectric interface as shown in Fig. 14.2. This is done in order to increase the accuracy of the boundary conditions and to avoid the problem of singularities of the field at the inner corners and edges.

The electric and magnetic potentials at the i^{th} node are Φ_i and Θ_i respectively. The differential equations are now reduced to their finite difference approximations. This is done by replacing the Laplacian operator by the well known five point approximation obtained using a Taylor series expansion. This gives

$$-(\frac{1}{h_x^2})[\Phi_n + \Phi_s + R^2\Phi_e + R^2\Phi_w] + (\frac{1}{h_x^2})[1 + R^2]\Phi_p = k_c^2\Phi_p \tag{32}$$

$$-(\frac{1}{h_x^2})[\Theta_n + \Theta_s + R^2\Theta_e + R^2\Theta_w] + (\frac{1}{h_x^2})[1 + R^2]\Theta_p = k_c^2\Theta_p \tag{33}$$

where h_x and h_y are the step sizes in the x and y directions respectively. R is the ratio of h_x to h_y. The subscripts n, s, e, w represent the nodes to the north, south, east and west of node P respectively as, shown in Fig. 14.3. A set of $2N$ equations are obtained.

For nodes on the metalic walls, the boundary conditions reduce to,

$$\Phi_{ni} = \Phi pi \tag{34}$$

$$\Theta_{ni} = \Theta pi \tag{35}$$

These are accurate to the order of h^2 where h is the step size of the grid.

On dielectric to dielectric interfaces the boundary conditions are obtained by using the idea of virtual points introduced by Collins and Dally [12]. This yields,

$$R(\alpha_i - \alpha_{i+1})(\theta_e - \theta_w) = \tau_i\phi_n^{(i)} - \tau_i\phi_s^{(i)v} - \tau_{i+1}\phi_n^{(i+1)v} + \tau_{i+1}\phi_s^{(i+1)} \tag{36}$$

$$R(\tau_i - \tau_{i+1})(\phi_e - \phi_w) = -\alpha_i\theta_n^{(i)} + \alpha_i\theta_s^{(i)v} + \alpha_{i+1}\theta_n^{(i+1)v} - \alpha_{i+1}\theta_s^{(i+1)} \tag{37}$$

Where $\alpha_i = \tau_i\epsilon_i$ and i is the upper dielectric and $i+1$ is for the lower dielectric. The superscript v stands for a virtual point. After the boundary condition equations (36) and (37) are used to modify (32) and (33) one obtains a new version of the discrete wave equation for the points on the dielectric to dielectric interface as

$$\frac{1}{2h_x^2}\{R(\alpha_i - \alpha_{i+1})\theta_e - R(\alpha_i - \alpha_{i+1})\theta_w + 2(1+R^2)(\tau_i + \tau_{i+1})\phi_p - 2\tau_i\phi_n - 2\tau_{i+1}\phi_s - R^2(\tau_i + \tau_{i+1})\phi_e - R^2(\tau_i + \tau_{i+1})\phi_w\} = k_{co}^2\phi_p \tag{38}$$

$$\frac{1}{h_x^2(\epsilon_i + \epsilon_{i+1})}\{-R(\tau_i - \tau_{i+1})\phi_e + R(\tau_i - \tau_{i+1})\phi_w + 2(1+R^2)(\alpha_i + \alpha_{i+1})\theta_p - 2\alpha_i\theta_n - 2\alpha_{i+1}\theta_s - R^2(\alpha_i + \alpha_{i+1})\theta_e - R^2(\alpha_i + \alpha_{i+1})\theta_w\} = k_{co}^2\theta_p \tag{39}$$

Now we have a set of $2N$ equations. In matrix form this is

$$AX = \lambda X \tag{40}$$

Hence the problem of finding β reduces to solving the eigenvalue problem. This problem is further simplified because it is possible to find a matrix B such that

$$S = BA \tag{41}$$

is symmetric. Pre-multiplying this equation by B, we get

$$BAX = SX = \lambda BX \tag{42}$$

It can be shown that a matrix P given by

$$P = D^{-1}SD^{-1} \tag{43}$$

Where $B = D^2$, has the same eigenvalues as matrix A. It is also seen that P is always symmetric. The problem is solved by applying the conjugate gradient method to the symmetric matrix P.

14.4 Conjugate Gradient Method [18]

In order to solve the eigenvalue problem defined in the section 3, which is of the form

$$AX = \lambda X \tag{44}$$

we consider the functional (refer [17])

$$F(X) =< AX; X >= X^T AX \tag{45}$$

subject to the constraint

$$< X; X >= X^T X = 1 \tag{46}$$

For TE and TM modes, A is either positive or negative semidefinite and minimization of (45) makes sense. Let Y denote the normalised form of X,

$$Y = \frac{X}{< X; X >} = \frac{X}{(X^T X)} \tag{47}$$

So,

$$F(Y)|_{min} =< AY; Y > |_{min} = \left.\frac{< AX; X >}{< X; X >}\right|_{min} = \lambda_{min} \tag{48}$$

Starting with an initial guess $X'(0)$ for the solution and orthogonalizing it to all the previously found eigenvectors, obtain $X(0)$. This is done to ensure that the eigenvalue does not converge to one which was obtained earlier.Thus the first approximation for the minimum eigenvalue is found using

$$\lambda(0) = F[Y(0)] =< AY(0); Y(0) > \tag{49}$$

The residual is calculated as

$$R(0) = \lambda(0)X(0) - AX(0) \tag{50}$$

Successive approximations to X are developed by choosing the directional vector $P(k)$ to be orthogonal to all the previous vectors. So,

$$X(k+1) = X(k) + t(k)P(k) \tag{51}$$

where

$$t(k) = \frac{-B \pm \sqrt{B^2 - 4AC}}{2A} \tag{52}$$

$$A = P_b(k)P_c(k) - P_a(k)P_d(k) \tag{53}$$

$$B = P_b(k) - \lambda(k)P_d(k) \tag{54}$$

$$C = P_a(k) - \lambda(k)P_c(k) \tag{55}$$

$$P_a(k) = \frac{< P(k); AX(k) >}{< X(k); X(k) >} \tag{56}$$

$$P_b(k) = \frac{< P(k); AP(k) >}{< X(k); X(k) >} \tag{57}$$

$$P_c(k) = \frac{< P(k); X(k) >}{< X(k); X(k) >} \tag{58}$$

$$P_d(k) = \frac{< P(k); P(k) >}{< X(k); X(k) >} \tag{59}$$

$$\lambda(k) = \frac{< AX(k); X(k) >}{< X(k); X(k) >} \tag{60}$$

It can be shown that the solution does converge because

$$F[Y(k+1)] - F[Y(k)] < 0 \tag{61}$$

The new eigenvalues are found using the relation

$$\lambda(k+1) = \frac{< AX(k+1); X(k+1) >}{< X(k+1); X(k+1) >} \tag{62}$$

The new residual is calculated using

$$R'(k+1) = \lambda(k+1)X(k+1) - AX(k+1) \tag{63}$$

Iterations are carried out until the following conditions are met:

$$\left|\frac{[\lambda(k+1)-\lambda(k)]}{\lambda(k+1)}\right| < tolerance_1 \tag{64}$$

$$||R'(k+1)|| < tolerance_2 \tag{65}$$

Then $R(k+1)$ is obtained by orthogonalising $R(k+1)$ in order to keep $X(k+1)$ orthogonal to the previously found eigenvectors.

In order to obtain $P(k+1)$ orthogonal to $P(k)$, we find

$$< P(k+1); HP(k) >= 0 \tag{66}$$

where H is defined by

$$H[X(k)-X(k+1)] = R(k)-R(k+1) \tag{67}$$

We could then find

$$q(k) = \frac{< r(k+1)-r(k); R(k+1) >}{< r(k+1)-r(k); P(k) >} \tag{68}$$

where

$$r(k) = \frac{R(k)}{< R(k); R(k) >} \tag{69}$$

Hence we have

$$P(k+1) = R(k+1) + q(k)P(k) \tag{70}$$

Subsequent eigenvalues are found by once agian making an initial guess for the eigenvector and then orthogonalising it to the previously found eigenvectors. Then proceeding on the same lines as before to find the eigenvalue. Thus all the desired eigenvalues and eigenvectors are found.

14.5 Numerical Results and Discussion

Initially, the case of hollow rectangular waveguides were solved. This was done because we could obtain analytical results to verify the

MODE(nm)	k^*_{cnm}	k^{**}_{cnm}	% diff	no. of iter	cpu time(sec)
10	0.7854	0.7853	0.006	385	144.2
01	1.0472	1.0471	0.011	753	315.7
11	1.3090	1.3089	0.010	1172	555.8
20	1.5708	1.5704	0.026	1070	558.4
21	1.8879	1.8875	0.021	1298	742.5
02	2.0944	2.0934	0.046	5067	1952.3

* theoretical ** calculated using 4800 nodes.

Table 14.1 Results for hollow rectangular waveguide, TE modes.

validity of the finite difference and conjugate gradient method. Solutions for L-shaped, single ridge, vaned rectangular, T-septate and co-axial rectangular waveguides were solved for TE and TM modes. Dispersion curves were plotted for the first few modes of various configurations of dielectric loaded waveguides, shielded microstrip lines, finlines and slotlines. These are discribed in the sections below.

14.5.1 Hollow Waveguides

Several hollow waveguide structures shown in Fig. 14.5 have been analysed. These results have been compared to analytical solutions. In all cases the results compare with a great degree of accuracy.

a. Hollow Rectangular Waveguide

The finite difference/conjugate gradient method was applied to obtain the modes of an hollow rectangular waveguide. It was found that the difference between the analytical solution and this method for any mode was 0.052%. This includes both discretization and computational errors.

The results for the rectangular waveguide for the TE and TM modes are given in Table 14.1 and Table 14.2 respectively. The number of iterations required for convergence to each eigen value as well as the CPU time for all the computations carried out on a VAX 8810 is presented.

MODE(nm)	k_{cnm}^{*}	k_{cnm}^{**}	% diff	no. of iter	cpu time(sec)
11	1.3090	1.3089	0.009	80	255.0
21	1.8879	1.8875	0.021	443	164.4
12	2.2368	2.2359	0.041	411	173.1
31	2.5784	2.5771	0.050	224	106.2
22	2.6180	2.6170	0.039	374	194.6
32	3.1525	3.1508	0.054	802	457.7

* theoretical ** calculated using 4800 nodes.

Table 14.2 Results for hollow rectangular waveguide, TM modes.

MODE	k_c	no. of iter	cpu time(sec)
1.	2.4238	418	38.0
2.	3.7587	1005	103.6
3.	6.2767	174	20.2
4.	6.2767	1340	172.0
5.	6.7436	447	63.1
6.	7.0791	991	151.0

Table 14.3 Results for L-shaped waveguide, TE modes.

b. L-Shaped Waveguide

Tables 14.3 and 14.4 describe the cutoff wavenumbers for the first six TE and TM modes of the L-shaped waveguide respectively. The finite difference method was applied to the L-shaped waveguide shown in Fig. 14.5b, with 1200 nodes.

This compared well with the result published by Reid and Walsh [7] with the difference of 0.46%. Looking at Table 14.5 we may notice that the degeneration of the third and fourth mode were not overlooked by this method.

MODE	k_c	no. of iter	cpu time(sec)
1.	6.1923	75	6.0
2.	7.7889	1240	111.4
3.	8.8766	97	9.7
4.	10.8457	1267	144.1
5.	11.2559	92	11.8
6.	12.8245	321	45.1

Table 14.4 Results for L-shaped waveguide, TM modes.

MODE	k_c	no. of iter	cpu time(sec)
1.	2.2469	586	107.7
2.	4.8476	528	111.7
3.	6.4491	712	168.4
4.	7.5175	1813	474.2
5.	9.8163	1857	534.9
6.	12.5534	2802	961.2

Table 14.5 Results for single ridge waveguide, TE modes.

c. Single Ridge Waveguide

The cutoff wavenumbers for the first six wavenumbers of the TE and TM modes for the single ridge waveguide shown in Fig. 14.5c are tabulated in Table 14.5 and Table 14.6 respectively. The solution was obtained using 2400 nodes. The results obtained agree well with those published by Speilman and Harrington [8], Beaubien and Wexler [2] [10], Bates and Ng [1] with a difference of less than 0.7%.

MODE	k_c	no. of iter	cpu time(sec)
1.	12.1032	112	17.6
2.	12.3846	345	63.5
3.	13.9926	336	71.1
4.	15.5777	541	127.0
5.	16.6335	141	37.3
6.	17.7533	358	104.4

Table 14.6 Results for single ridge waveguide, TM modes.

MODE	k_c	no. of iter	cpu time(sec)
1.	1.5707	3453	872.3
2.	2.0752	266	75.2
3.	3.1408	682	218.0
4.	3.3028	385	134.4
5.	4.2489	2448	951.9
6.	4.7097	2184	920.4

Table 14.7 Results for vaned rectangular waveguide, TE modes.

The results obtained for the same case are as follows.

k_c for the dominant TE mode = 2.2566 (Speilman and Harrington) [8]
2.250 (Bates and Ng) [1]
2.412 (Beaubien and Wexler) [2]
2.2627 (Bulley and Davies) [3]

k_c for the dominant TM mode = 12.164 (Spielman and Harrington) [8]
12.141 (Beaubien and Wexler) [2]
12.134 (Bates and Ng) [1]

MODE	k_c	no. of iter	cpu time(sec)
1.	3.6855	120	25.7
2.	4.9515	242	62.2
3.	6.4418	238	67.8
4.	6.4703	352	111.4
5.	7.0187	300	105.3
6.	7.7294	223	87.3

Table 14.8 Results for vaned rectangular waveguide, TM modes.

d. Vaned Rectangular Waveguide.

Table 14.7 and Table 14.8 show the cutoff wavenumbers for the first six TE and TM modes of vaned rectangular waveguide (Fig. 14.5d) respectively. The solution was obtained using 3200 nodes. The difference between the result obtained and those published by Silvester is 2.55%.

e. T-Septate Waveguide

The finite difference, conjugate gradient solution for a T-septate waveguide shown in Fig. 14.5e was solved using 2880 nodes. The cutoff wavenumbers for the first six TE and TM modes are given in Table 14.9 and Table 14.10 respectively. The largest difference between this solution and that given by Beaubien and Wexler is 1.73%.

f. Coaxial Rectangular Waveguide

Table 14.11 and Table 14.12 give the waveguide cutoff numbers for the first six TE and TM modes respectively of the coaxial rectangular waveguide shown in Fig. 14.5f.

14.5.2 Dielectric Loaded Waveguides

In this section the dispersion characteristics for the transmission line structures shown in Fig. 14.6 (all dimensions in centimeters) are computed. The normalised propagation constant $\overline{\beta}$ has been plotted

MODE	k_c	no. of iter	cpu time(sec)
1.	2.9176	916	205.4
2.	3.0328	500	127.1
3.	5.5353	259	74.2
4.	7.2295	2416	776.6
5.	8.8832	1195	419.7
6.	11.3194	439	166.5

Table 14.9 Results for T-septate waveguide, TE modes.

MODE	k_c	no. of iter	cpu time(sec)
1.	8.1336	120	22.1
2.	10.8825	404	89.8
3.	14.3273	209	53.0
4.	14.5453	499	141.2
5.	16.2067	3065	974.2
6.	18.0186	3124	1022.3

Table 14.10 Results for T-septate waveguide, TM modes.

as a function of the normalised frequency, giving us the dispersion curves. These results obtained are almost identical with those presented by Manela [20], within plotting accuracy. Observe that in this case, the modes can cross each other. This is because of the fact that the eigenvectors corresponding to different propagation constants are not orthogonal for an unsymmetric matrix.

14.5.3 Finlines and Slotlines

Here, several structures like the centered dielectric slab waveguide, unilateral finline, bilateral finline, unilateral slotline etc. shown in Fig. 14.7 have been analysed. The dispersion curves $\overline{\beta}$ as a function of normalised cutoff wavelengths have been plotted. When available these

MODE	k_c	no. of iter	cpu time(sec)
1.	2.0443	544	77.0
2.	2.8222	334	53.1
3.	3.9591	2055	371.7
4.	5.1316	1848	374.1
5.	5.7189	1945	435.4
6.	6.3892	964	230.5

Table 14.11 Results for coaxial rectangular waveguide, TE modes.

MODE	k_c	no. of iter	cpu time(sec)
1.	6.8121	68	8.4
2.	6.8586	274	38.4
3.	8.3556	218	35.3
4.	8.5196	291	52.5
5.	10.3111	106	21.7
6.	10.8633	260	57.6

Table 14.12 Results for coaxial rectangular waveguide, TM modes.

have been compared to published results.

a. Centered Dielectric Waveguides

Two centered dielectric waveguides shown in Figs. 14.7a and 14.7d analysed by this method compare well with published results. The difference is well within plotting accuracy. In case of Fig. 14.7a, the results from Harrington [19] and Manela [20] show a very close proximity to the results obtained here. In the case of Fig. 14.7d, the results compare very well with those published by Schmidt and Itoh [15].

b. Finlines

Using this method of analysis, the dispersion curves for the uni-

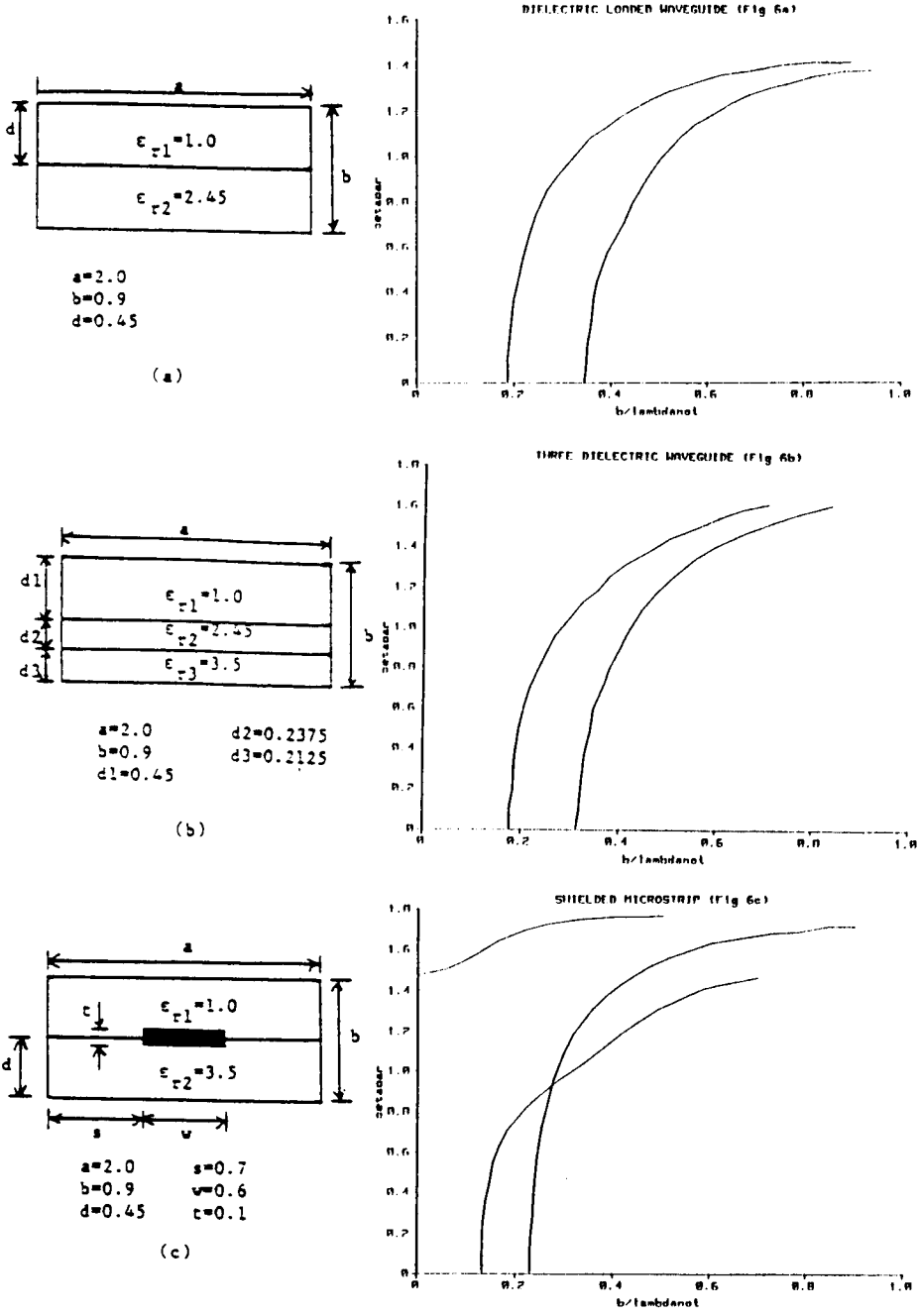

Figure 14.6 Continued on next page.

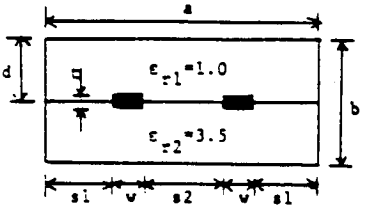

a=2.0 s1=0.5 t=0.047
b=0.9 s2=0.6
d=0.45 w=0.2

(d)

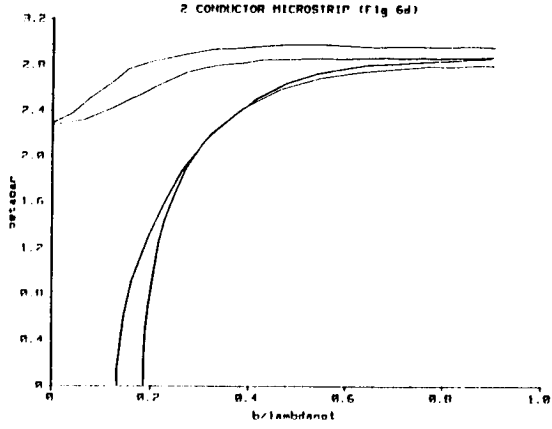

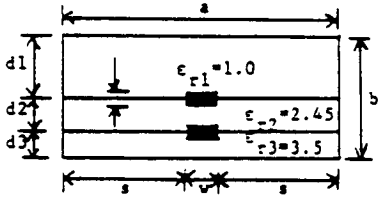

a=2.0 d2=0.2375 s=0.9
b=0.9 d3=0.2125 t=0.047
d1=0.45 w=0.2

(e)

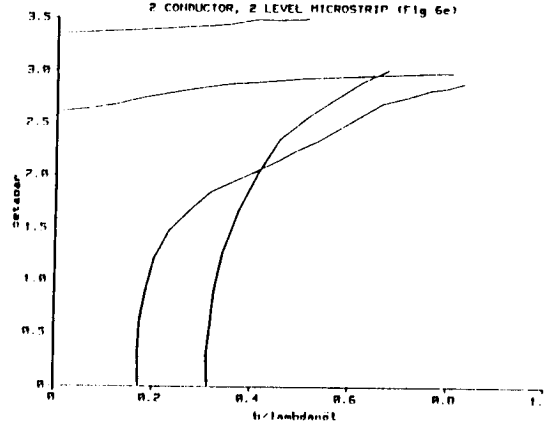

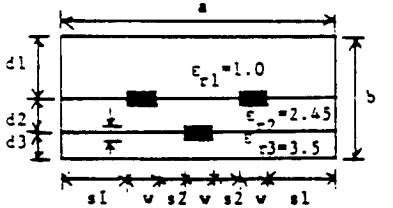

a=2.0 d2=0.2375 s1=0.5
b=0.9 d3=0.2125 s2=0.2
d1=0.45 w=0.2 t=0.047

(f)

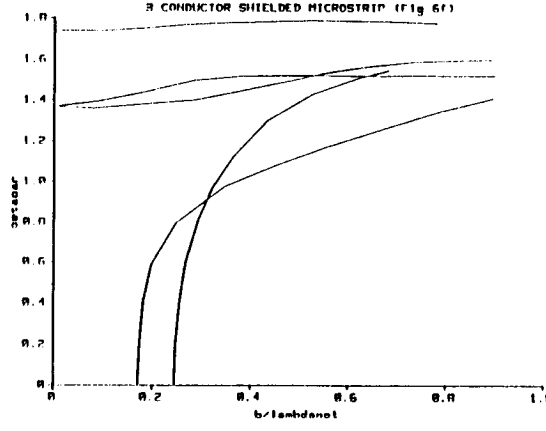

Figure 14.6 (a) Dielectric loaded waveguide, (b) Three dielectric waveguide, (c) Single conductor shielded line, (d) Two conductor shielded line, (e) Two conductor, two level shielded line, (f) Three conductor line.

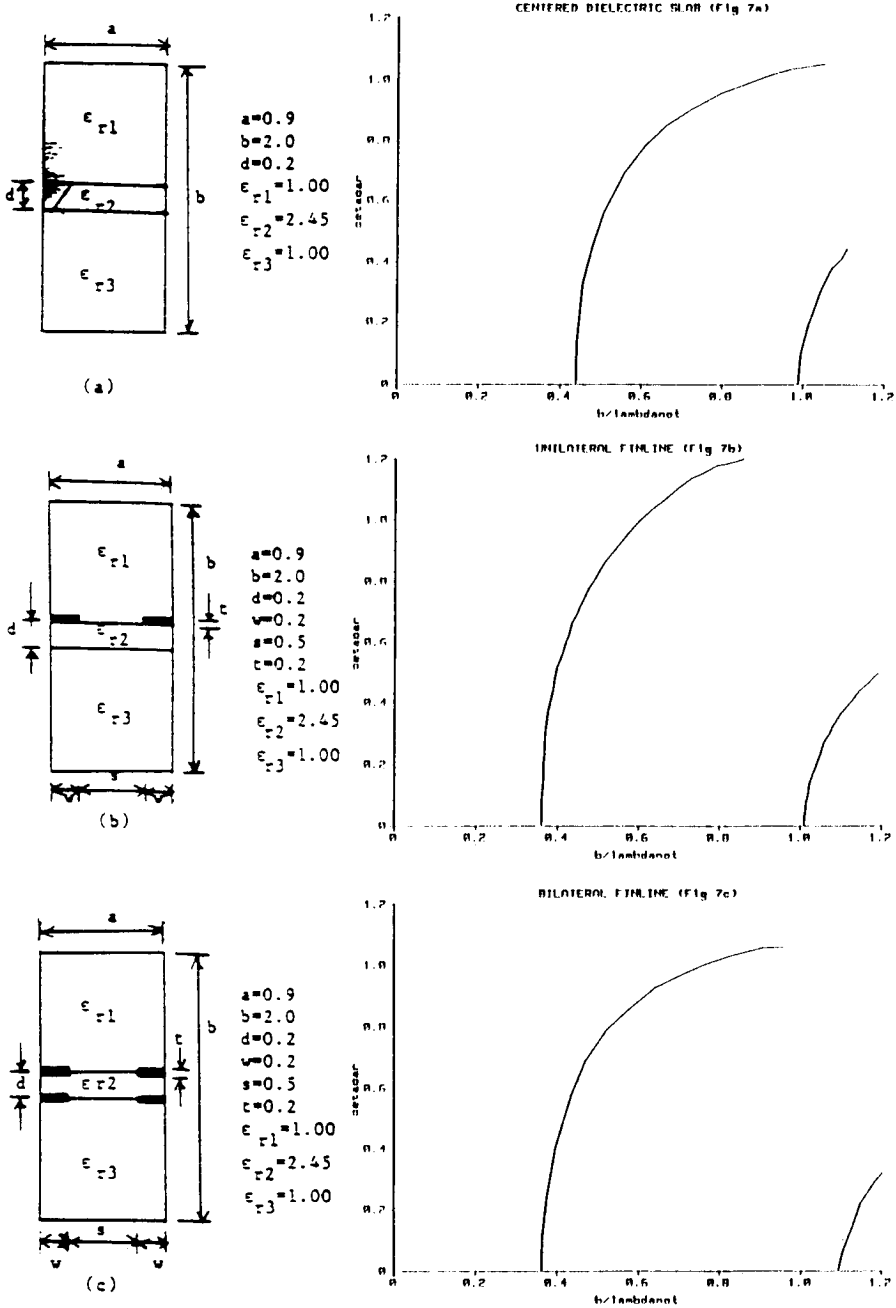

Figure 14.7 Continued on next page.

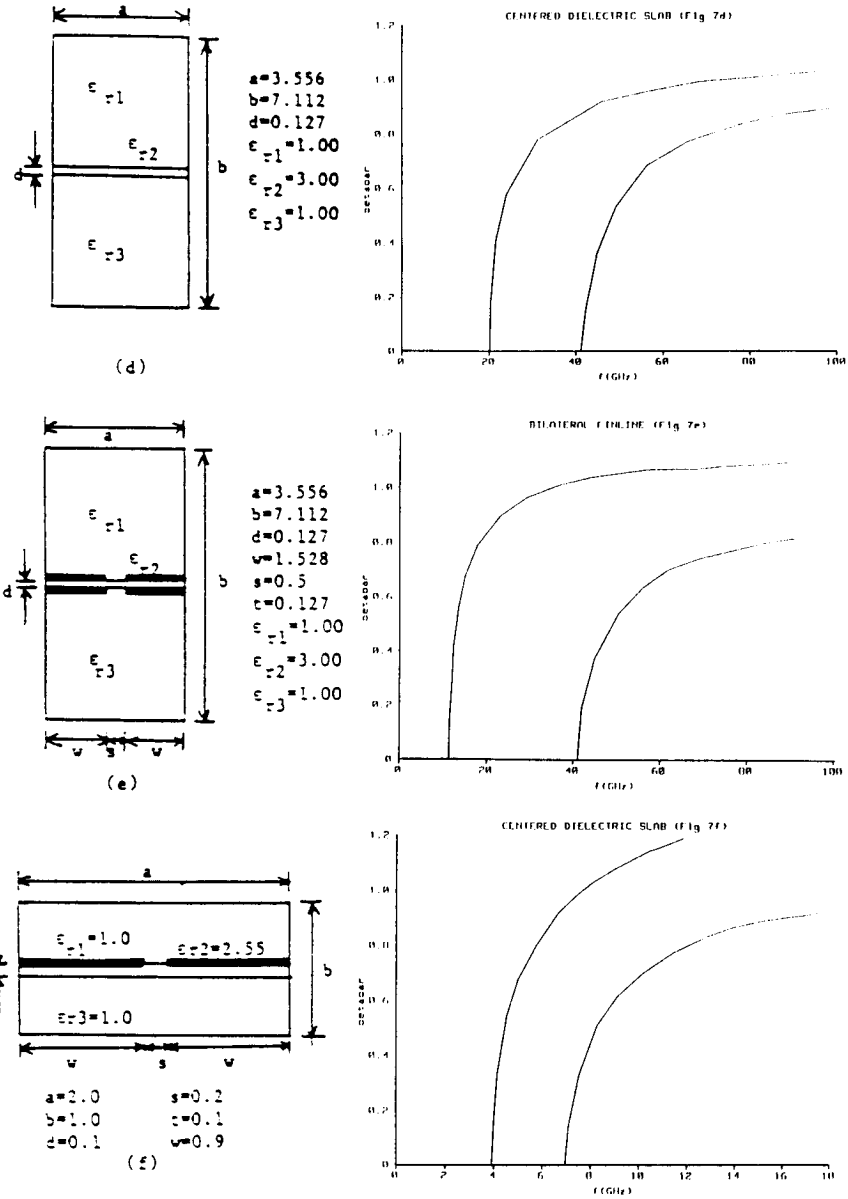

Figure 14.7 Configurations considered in section 14.5.3 (a) Rectangular waveguide with centered dielectric slab, (b) Unilateral finline, (c) Bilateral finline, (d) Rectangular waveguide with centered dielectric slab, (e) Bilateral finline, (f) Unilateral slotline.

lateral and bilateral finlines shown in Figs. 14.7b, 14.7c and 14.7e have been plotted and it has been observed that these results are in agreement with those published by Schmidt and Itoh [15].

c. Slotline

The structure whose cross-section has been shown in Fig. 14.7f has been analysed. Yamashita and Atsuki [16] have published results for the same structure. A close agreement has been observed between the two results.

14.6 Conclusions

As shown by comparison of data (when available), this method is very accurate and dependable. As shown in the numerical results section, the procedure can be applied to a variety of problems with equal success. This method is quite fast and accurate because the physical problem can transferred into an eigenvalue problem of a symmetric matrix which can be solved efficiently using the conjugate gradient method. This application of the conjugate gradient method takes advantage of the sparseness of the matrix resulting from the finite difference approximation, saving considerable computer time and storage. The computer storage is only $16 \times N$ rather than N^2 (where N is the dimension of the matrix to be solved). Much computer time is also saved because the conjugate gradient method enables the first few eigenvalues and corresponding eigenvectors to be found without searching for all N of them.This method has a big advantage over the nonsymmetric formulation used in [20] in that the conjugate gradient method can be used to solve the matrix eigenvalue problem. Now a much greater number of nodes can be used to reduce the discretization error.

References

[1] Bates, R. H., and F. L. Ng.,"Point matching Computation of transverse resonance," *Int. J. Num. Meth. Eng.*, **6**, 155–168, 1973.

[2] Beaubien, M. H., and A. Wexler, "An accurate finite difference method for higher order waveguide modes," *IEEE Trans. Microwave Theory Tech.,* (1968 Symposium issue) **16,** 1007–1017, Dec. 1968.

[3] Bulley, R. M., and J. B. Davis, "Computation of approximate polynomial solutions to TE modes in an arbitrary shaped waveguide," *IEEE Trans. Microwave Theory Tech.,* (special issue on computer-oriented microwave practices) **17,** 440–446, Aug. 1969.

[4] Ng, F. L., "Contributions to guided wave theory," *Ph.D. Dissertation,* Dept. Elec. Eng., Univ. Canterbury, Christchurch, New Zealand.

[5] Ng, F. L., "Tabulation of the methods for the numerical solution of the hollow waveguide problem," *IEEE Trans, Microwave Theory Tech.,* **22,** 322–329, March 1974.

[6] Gruner, L., "Higher order modes in rectangular coaxial waveguides," *IEEE Trans. Microwave Theory Tech.,* (corresp), **MTT-15,** 483–485, August 1967.

[7] Reid, J. K., and J. E., Walsh, "An elliptic eigenvalue problem for a reentrant region," *J. Soc. Ind. Appl. Math.,* **13,** 837–850, 1965.

[8] Spielman, B. E., and R. F. Harrington, "Waveguide of arbitrary cross section by solution of a nonlinear integral eigenvalue equation," *IEEE Trans. Microwave Theory Tech.,* **20,** 578–585.

[9] Silvester, P., "A general high order finite element waveguide analysis program," *IEEE Trans. Microwave Theory Tech.,* **17,** 204–210, April 1969.

[10] Beaubien, H. J., and A. Wexler, "Unequal arm finite difference operators," *IEEE Trans. Microwave Theory Tech.,* **MTT-18,** December 1970.

[11] Corr, D. G., and J. B., Davies, "Computer analysis of the fundamental and higher order modes in single and coupled microstrips," *IEEE Trans. Microwave Theory Tech.,* **MTT-20,** October 1972.

[12] Collins, J. B., and P. Daly, "Calculation for guided electromagnetic wave using finite difference methods," *J. of Electronic control,* **14,** 361–380, 1963.

[13] Hornsby, J. S., and A. Gopinath, "Numerical analysis of dielectric

loaded waveguides with a microstrip line - finite difference models," *IEEE Trans. Microwave Theory Tech.*, **MTT-17**, September 1969.

[14] Schweig, E., and W. B., Bridges, "Computer analysis of dielectric guides, a finite difference model," *IEEE Trans. Microwave Theory Tech.*, **MTT-32**, May 1984.

[15] Schmidt, L. P., and T. Itoh, "Spectral domain analysis of dominant and higher order modes in fin-lines," *IEEE Trans. Microwave Theory Tech.*, **MTT-28**, September 1980.

[16] Yamashita, E., and K. Atsuki, "Analysis of microstrip like transmission lines by nonuniform discretization of integral equations," *IEEE Trans. Microwave Theory Tech.*, April 1986.

[17] Kantarovich, L. V., "Functional analysis and applied mathematics," *Uspekhi Matematicheskie Naum*, **3**, No. 6, 89–185, 1948.

[18] Yang, X., T. K. Sarkar, and E. Arvas, "A survey of Conjugate gradient algorithms for extreme eigen-problems of a symmetric matrix," *IEEE Trans. Acoustic, Speech, Signal Processing*, **ASSP-37** 1550–1556, October 1989.

[19] Harrington, R. F., *Time Harmonic Electromagnetic Fields* New York, McGraw Hill, 1961.

[20] Manela, M., "Finite difference treatment of dielectric loaded wave -guides and shielded microstrips," *Ph.D thesis*, Syracuse University, December 1988.

[21] Sarkar, T. K., K. Athar, E.Arvas, M. Manela, and R. Lade, "Computation of propagation characteristics of TE and TM modes in Arbitrary shaped Hollow Waveguides Utilizing the Conjugate Gradient method," *Journal of Electromagnetic Waves and Applications*, **3**, No. 2, 143–165, 1989.